MIMO sonar systems for harbour surveillance

Yan Pailhas
and Yvan Petillot
Ocean Systems Lab, School of EPS
Heriot Watt University
Edinburgh, Scotland, EH14 4AS
Email: Y.Pailhas@hw.ac.uk

***Abstract*—Multiple Input Multiple Output sonar systems offer new perspectives for target detection and area surveillance. This paper introduces MIMO sonar systems and focuses on its capabilities. The multiplication of the number of transmitters and receivers not only provides a greater variety in terms of target view angles but provides also in meaningful statistics on the target itself. Assuming that views are independent and the MIMO system is large enough we demonstrate that target recognition is possible with only one view from the full system. We also demonstrate that such systems solve the speckle target noise and decorrelate individual scatterers within one cell resolution. We show that MIMO systems can achieve super-resolution images and surpass the resolution given by equivalent SAS (Synthetic Aperture Sonar) systems. To demonstrate those capabilities we develop a physic based MIMO simulator capable of modelling cluttered and very shallow marine environment similar of harbour environment. Thanks to the simulator and taking advantage of the degree of freedom that MIMO systems offers, we also present autofocus algorithms that automatically estimates mid-water target parameters such as speed, orientation or depth.**

I. Introduction

MIMO stands for Multiple Input Multiple Output. MIMO generally refers to a system with several transmitters and several receivers. Such systems can been seen as a variety of multi-static systems, the main difference being that MIMO system has the capability to process the information as a whole while multi-static systems only process the data at the receiver nodes. This implies that there is an overall strategy for MIMO systems, a strategy specific to the end application. We can distinguish two levels of freedom in MIMO systems, the first one being at the transmitter level. The classic approach is to consider orthogonal waveforms in order to separate the bistatic signals from all the different transmitters. Finite orthogonal waveforms do not exist and the search for approximate orthogonal waveforms is an active subject of research. The other level of freedom is at the receiver end and different techniques can be designed to extract target information from the $K \times L$ signals (where K is the number of transmitters and L the number of receivers).

MIMO systems have received a lot of interest in recent years in the radar community [1]. Radar researchers have pointed out multiple advantages of these systems such as diversity gain for target detection [2], angle of arrival [3] or Doppler estimation [4]. Despite their great potential, sonar MIMO systems have rarely been considered for surveillance purposes.

In this paper we are interested in the problem of harbour surveillance. Multiple Inout Multiple Output (MIMO) sonar systems can offer great capabilities for area surveillance especially in very shallow water with heavy cluttered environment such as harbour environment thanks to their enhanced spatial diversity. To benefit from the view diversity MIMO systems with spatially distributed transmitters and receivers are considered. A full 3D MIMO simulator is presented, which can compute synthetic raw data for any transmitter/receiver pair in a multipath and cluttered environment. Synthetic seabed interfaces are computed using 2D fractional Brownian motion. Bistatic reverberation levels are computed using the physical model developed by APL-UW [5]. Finally the mirror theorem is used to compute the various multipaths. Synthetic mid-water targets can also be added to the environment. Simulating sound propagation in 3D can be computationally expensive but this cost can be reduced using sparse techniques. Results in simulation are presented and show that with careful configuration of the MIMO elements, super resolution imaging and speckle resolution can be achieved. We also demonstrate that autofocus techniques can be used to estimate target depth and velocity in complex scenarios.

The paper is organised as follow: in section II-A we present the notations and MIMO formulations we will be using in this paper. In section II-B and II-C we derive the main properties for large MIMO sonar systems. We demonstrate here the automatic target recognition (ATR) capabilities and the super-resolution capability of MIMO sonar systems. In section III, we describe the physical based MIMO simulator. Finally in section IV we present two autofocus algorithms using MIMO system to estimate depth, speed and orientation of a mid-water target in complex environment.

II. MIMO sonar systems: notations and properties

A. MIMO sonar formulation

The first formulation for surveillance MIMO systems has been made by the radar community [1]. We present here the most popular model for a radar target model. the finite scatterer model used in [6], [7]. A target is represented here with Q scattering points spatially distributed. Let $\{X_q\}_{q\in[1,Q]}$ be their locations. The reflectivity of each scattering point is represented by the complex random variable ζ_q. All the ζ_q are assumed to be zero-mean, independent and identically distributed with a variance of $E[|\zeta_q|^2] = 1/Q$. Let Σ be the

reflectivity matrix of the target, $\Sigma = \text{diag}(\zeta_1, ..., \zeta_Q)$. By using this notation the average RCS (radar cross section) of the target $\{X_q\}$, $E[\text{tr}(\Sigma\Sigma^H)]$, is normalised to 1.

The MIMO system comprises a set of K transmitters and L receivers. Each transmitter k sends a pulse $\sqrt{E/K}.s_k(t)$. We assume that all the pulses $s_k(t)$ are normalised. Then E represents the total transmit energy of the MIMO system. Receiver l receives from transmitter k the signal $z_{lk}(t)$ which can be written as:

$$z_{lk}(t) = \sqrt{\frac{E}{K}} \sum_{q=1}^{Q} h_{lk}^{(q)} s_k \left(t - \tau_{tk}(X_q) - \tau_{rl}(X_q)\right) \quad (1)$$

with $h_{lk}^{(q)} = \zeta_q \exp\left(-j2\pi f_c[\tau_{tk}(X_q) + \tau_{rl}(X_q)]\right)$. f_c is carrier frequency, $\tau_{tk}(X_q)$ represents the propagation time delay between the transmitter k and the scattering point X_q, $\tau_{rl}(X_q)$ represents the propagation time delay between the scattering point X_q and the receiver l. Note that $h_{lk}^{(q)}$ represents the total phase shift due to the propagation and the reflection on the scattering point X_q.

Assuming the Q scattering points are close together (*i.e.* within a resolution cell), we can write:

$$\begin{aligned} s_k \left(t - \tau_{tk}(X_q) - \tau_{rl}(X_q)\right) &\approx s_k \left(t - \tau_{tk}(X_0) - \tau_{rl}(X_0)\right) \\ &= s_k^l(t, X_0) \end{aligned} \quad (2)$$

where X_0 is the centre of gravity of the target $\{X_q\}$. So Eq. (1) can be rewritten as:

$$\begin{aligned} z_{lk}(t) &= \sqrt{\frac{E}{K}} s_k^l(t, X_0) \times \\ &\quad \left(\sum_{q=1}^{Q} \zeta_q \exp\left(-j2\pi f_c[\tau_{tk}(X_q) + \tau_{rl}(X_q)]\right)\right) \\ &= \sqrt{\frac{E}{K}} \left(\sum_{q=1}^{Q} h_{lk}^{(q)}\right) s_k^l(t, X_0) \end{aligned} \quad (3)$$

B. ATR capabilities

In this section we are interested in the MIMO intensity response of an object: $\sum_{q=1}^{Q} h_{lk}^{(q)}$ from Eq. (3). Lets assume that the reflectivity coefficients ζ_q can be modelled by the random variable $\frac{1}{\sqrt{Q}} e^{2i\pi U}$ where $U \in [0, 1]$ is the uniform distribution. The central limit theorem then gives us the asymptotic behaviour of the target intensity response, and we can write:

$$\lim_{Q \to +\infty} \sqrt{\left| \sum_{q=1}^{Q} h_{lk}^{(q)} \right|^2} = \text{Rayleigh}(1/\sqrt{2}) \quad (4)$$

The convergence of Eq. (4) is fast as shown in [8]. However for a small number of scatterers (typically $Q \leq 5$), the target reflectivity PDF exhibits noticeable variation from the Rayleigh distribution.

Assuming that man-made targets can be effectively modelled by a small number of scatterers, we can take advantage of the dissimilarities of the reflectivity PDF functions to estimate the number of scattering points. Each observation is a realisation of the random variable $\gamma_n = \sqrt{\left| \sum_{q=1}^{Q} h_{lk}^{(q)} \right|^2}$ with Q the number of scattering points. Each set of observations $\Gamma = \{\gamma_n\}_{n \in [1,N]}$ where N is the number of views represents the MIMO output. Given Γ, we can compute the probability that the target has Q scatterers using Bayes rules:

$$\text{P}(T_Q|\Gamma) = \frac{\text{P}(\Gamma|T_Q)\text{P}(T_Q)}{\text{P}(\Gamma)} \quad (5)$$

where T_Q represents the event that the target has Q scatterers. Assuming independent observations, we have:

$$\text{P}(\Gamma|T_Q) = \prod_{n=1}^{N} \text{P}(\gamma_n|T_Q) \quad (6)$$

We consider 4 target types: 2, 3, 4 and 5+ scatterer targets. With $Q \in \{2, 3, 4, 5+\}$, we can then expend $\text{P}(\Gamma)$ to:

$$\text{P}(\Gamma) = \sum_{Q=2}^{5} \text{P}(\Gamma|T_Q)\text{P}(T_Q) \quad (7)$$

Given that we have no *a priori* information about the target we can assume that $\text{P}(T_Q)$ is equal for all target class T_Q. Eq. (5) then becomes:

$$\text{P}(T_Q|\Gamma) = \frac{\prod_{n=1}^{N} \text{P}(\gamma_n|T_Q)}{\sum_{Q=2}^{5+} \text{P}(\Gamma|T_Q)} \quad (8)$$

The estimated target class corresponds to the class which maximises the conditional probability given by Eq. (8).

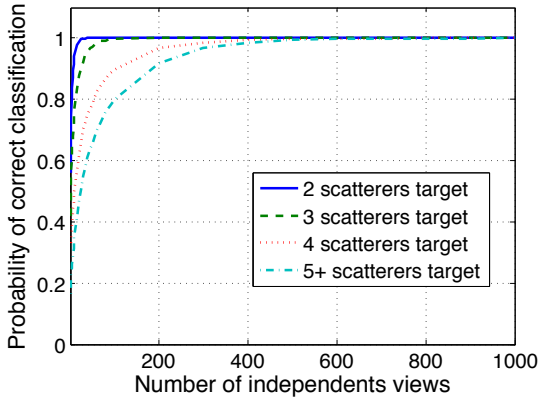

Fig. 1. Correct classification probability against the number of independent views for 4 classes of targets (2, 3, 4 and 5+ scattering points targets).

Figure 1 draws the probability of correct classification for each class depending on the number of views based on 10^6 classification experiments. Note that the simulations have been run with 10 dB SNR. The first observation we can make is that it is possible to estimate the number of scattering points for target with low number of scatterers by only observing the target echo amplitude for a sufficient number of views. With only 100 views, the overall probability of correct classification is great than 92%.

C. Super-resolution capabilities

In section II-B we show the ATR capabilities for large incoherent MIMO sonar systems. In this section, we demonstrate its super-resolution capabilities in terms of sonar imagery.

Let $r_l(t)$ be the total received signal at the receiver l. We can write $r_l(t) = \sum_{k=1}^{K} z_{lk}(t)$. The target response x_{lk} from the MIMO system is then the output of the filter bank $s_k^*(t)$ with $k \in [1, K]$. With our notations and assuming orthogonal waveforms, we arrive to:

$$x_{lk} = r_l \star s_k^*(t) = \sum_{q=1}^{Q} h_{lk}^{(q)} \tag{9}$$

The average target echo intensity from all the bistatic views is given by:

$$\mathcal{F}(\mathbf{r}) = \frac{1}{N} \sum_{l,k} ||x_{lk}||^2 \tag{10}$$

Using the same target probability distribution stated in the model presented earlier (cf. section II-A), we deduce that $\mathcal{F}(\mathbf{r})$ follows the probability distribution:

$$\mathcal{F}(\mathbf{r}) \sim \frac{1}{N} \sum_{n=1}^{N} \text{Rayleigh}^2(\sigma) \sim N.\Gamma(N, 2\sigma^2) \tag{11}$$

where Γ is the Gamma distribution. Note that the second equivalence is given using the properties of the Rayleigh distribution. The asymptotic behaviour of $\mathcal{F}(\mathbf{r})$ can be deduced from the following identity [9]:

$$\lim_{N \to +\infty} N.\Gamma(Nx, N, 1) = \delta(1 - x) \tag{12}$$

Eq. 12 shows that the MIMO mean target intensity $\mathcal{F}(\mathbf{r})$ converges toward the RCS defined in section II-A which means that the scatterers within one resolution cell decorrelate between each other. MIMO systems then solve the speckle noise in the target response. This demonstrates why super-resolution can be achieved with large MIMO systems.

In order to image the output of the MIMO system we will use the multi-static back- projection algorithm which is a variant of the bistatic back-projection algorithm developed by the Synthetic Aperture Radar (SAR) community. Further details can be found in [10]. Using the back-projection algorithm the Synthetic Aperture Sonar (SAS) image is computed by integrating the echo signal along a parabola. In the bistatic case the integration is done along ellipses. For the multi-static scenario the continuous integration is replaced by a finite sum in which each term corresponds to one transmitter/receiver pair contribution.

In the following simulation we aim to demonstrate that we can recover the geometry of a target (*i.e.* the location of its scatterers). We chose a "L" shape MIMO configuration: the transmitters are placed along the x-axis, the receivers along the y-axis. The MIMO system frequency band is 50 kHz to 150 kHz. We consider a 3 point scatterers target, the scatterers are separated by one wavelength. In figure 2(a) we consider a 10 Tx $\times$ 10 Rx MIMO system. With this configuration we are able to clearly image the 3 scatterer target in so doing achieve super resolution imaging. For comparison purposes we have computed the SAS image (cf. Fig. 2(b)) of the same target using the same frequency band and at the same range. The full geometry of the target is not recovered there.

III. MIMO SIMULATOR

In this section we describe the main components of the 3D MIMO sonar simulator.

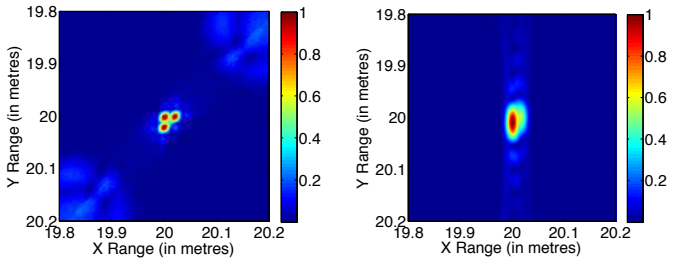

(a) (b)

Fig. 2. 3 scatterers target: (a) MIMO image using 10 transmitters and 10 receivers with 3 metres spacing, (b) SAS image.

A. Seabed interface

To model the seabed interface we generate 2D fractional Brownian motion (fBm) using the Incremental Fourier Synthesis Method developed by Kaplan and Kuo [11]. The main idea is to model the 1st and 2nd order increments I_x, I_y and I_2. I_x, I_y and I_2 are given by:

$$\begin{aligned} I_x(m_x, m_y) = &\quad B(m_x + 1, m_y) - B(m_x, m_y) \\ I_y(m_x, m_y) = &\quad B(m_x, m_y + 1) - B(m_x, m_y) \\ I_2(m_x, m_y) = &\quad B(m_x + 1, m_y + 1) + B(m_x, m_y) \\ &- B(m_x, m_y + 1) - B(m_x, m_y + 1) \end{aligned}$$

where B is the 2D fBm. Those 1st and 2nd order increments can be computed thanks to their FFTs. The 2nd order increment FFT is given by:

$$S_2(\omega_x, \omega_y) = \frac{32\sqrt{\pi} \sin^2(\omega_x/2) \sin^2(\omega_y/2) \Gamma(2H+1) \sin(\pi H)}{\sqrt{\omega_x^2 + \omega_y^2}^{2H+2}} \tag{13}$$

where H is the Hurst parameter. Figure 3 displays an example of 2D fBm surface generated using this technique.

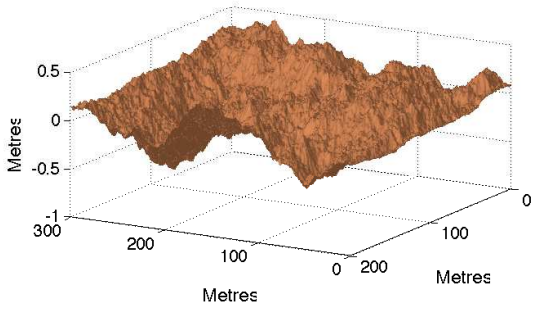

Fig. 3. Example of 2D fBm with H = 0.8 (fractal dimension = 2.2)

B. Bistatic reverberation level

The bistatic scattering strength is computed using the model developed by Williams and Jackson [5]. It is given by:

$$S_b(\theta_s, \phi_s, \theta_i) = 10 \log[\sigma_{br}(\theta_s, \phi_s, \theta_i) + \sigma_{bv}(\theta_s, \phi_s, \theta_i)] \tag{14}$$

where $\sigma_{br} = [\sigma_{kr}^{\eta} + \sigma_{pr}^{\eta}]^{1/\eta}$ is the bistatic roughness scattering which includes the Kirchhoff approximation and the perturbation approximation. σ_{bv} is the sediment bistatic volume scattering. S_b depends on the bistatic geometry as well as the sediment physical properties. Figure 4 displays the bistatic

scattering strength for a Tx/Rx pair situated 141m apart and both at 7.5m from the seafloor. The S_b is computed for two different sediment types (coarse sand and sandy mud) for the same fBm interface.

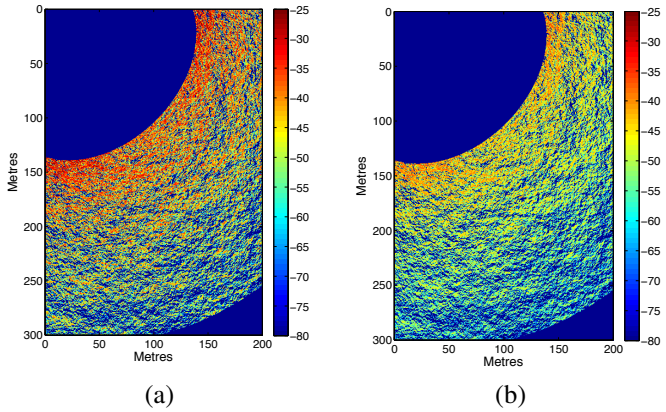

(a) (b)

Fig. 4. Bistatic scattering strength relative to one Tx located at [0m,100m] and a Rx located at [100m,0m] for (a) a coarse sand sediment type and (b) a sandy mud sediment type.

C. Propagation

Sound propagation in shallow water can become extremely complex. Because we are modelling very shallow water environment we assume a constant sound speed through the water column. To model the multipath we are using the mirror theorem. We use ray tracing techniques to compute the different propagation paths. The simulations done in this paper consider a maximum of three bounces.

To synthesise time echo a random scatterer point cloud including random position and random intensity is generated for each cell in the seabed. Note that once the point cloud is generated, it can be saved for other simulations with the same configuration.

To synthesise the MIMO echoes from a 200m $\times$ 300m scene with 50cm cell resolution we have to compute 400 $\times$ 600 cells $\times$ 20 scatterers per cell $\times$ 100 MIMO pairs different paths which represents around half a billion paths (direct paths only). Brute force computation using MatLab on a standard laptop requires around 2 months of computation. This can be drastically reduced by analysing the properties of propagation in water and the circular convolution properties of the DFT. The main tool to propagate a signal is free water is the well known FFT property: $f(t-u) \Leftrightarrow \mathrm{e}^{-iu\omega}\hat{f}(\omega)$. If we consider the echo related to one cell, this echo is extremely sparse over a 600m range signal. The idea is to compute the propagated signal over a much smaller window. Figure 5 draws the outlines of the algorithm: the full scene is divided into range bands, on Fig. 5(a) each colour band represents a 10m range division. The echoes relative to each band are computed independently on a small window of 20m (cf. figure 5(b)). The echoes are then recombined to give the full range bistatic response as seen in figure 5(c). Using those techniques greatly reduces the computation time from 2 months to few hours.

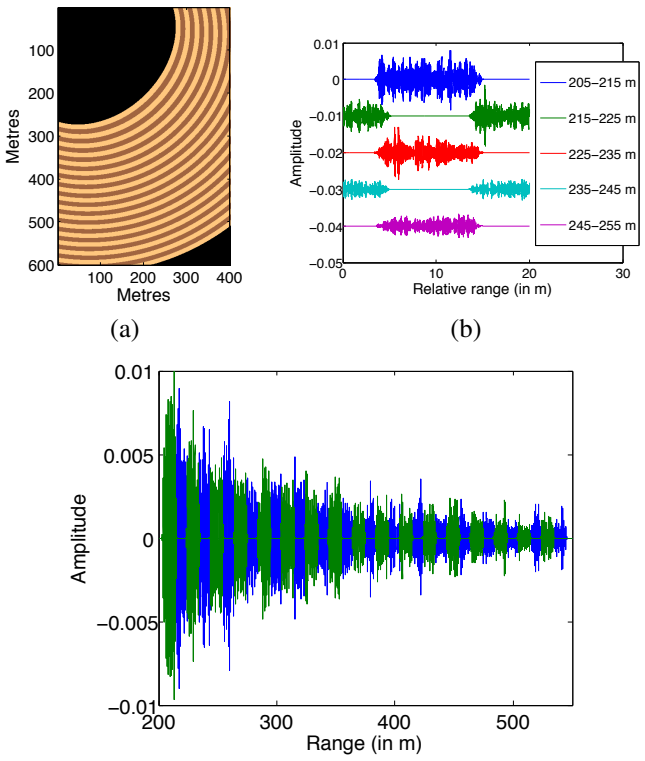

(a) (b) (c)

Fig. 5. (a) of the observed scene in 10m range band. (b) Individual range band echo contribution. (c) Full echo response recomposition.

IV. Autofocus with MIMO systems

The MIMO images are computed using the multistatic back projection algorithm which is a variant of the bistatic back projection algorithm [10] developed by the SAR community. For the multi-static scenario the continuous integration along ellipses is replaced by a finite sum in which each term corresponds to one transmitter/receiver pair contribution. In this section we propose two variants of the multistatic back projection algorithm to estimate the depth of a mid-water target, its speed and orientation.

A. Depth estimation

As it has been mentioned before synthetic aperture MIMO imaging shares a lot of features with standard SAS imaging. In particular the image is projected onto a plane or a bathymetry estimate representing the seafloor level. The image of a mid water target will then appear unfocused for this particular projection. By moving the projection plane through the water column the MIMO target image will focus at its actual depth. Using simple autofocus algorithm and maximising the target amplitude it is then possible to estimate the depth of the target even if the MIMO system is coplanar. For a mid-water target at 400 m range in a 15 m depth environment it is possible to estimate its depth with 10 to 50 cm accuracy. Figure 6 displays the autofocus results and the estimated target depth compared with the ground truth.

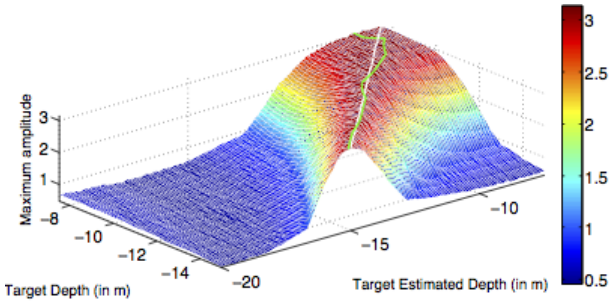

Fig. 6. Autofocus algorithm results based on maximising the scattering response: ground truth (white curve) and estimated depth (green curve).

B. Speed and direction estimation

Speed estimation for MIMO systems is an active subject of research in the radar community [12], [13] . Most of the proposed methods are based on maximum-likelihood (ML) estimation and then rely on the Doppler shift of the moving target. In our case we are interested in low velocity target (few knots) in a highly cluttered and multiplath environment. For these reasons we assume in this paper that the Doppler shift is negligible.

The main idea of speed and direction autofocus is to introduce a defocus for moving objects and then estimate the speed and direction parameter $\overrightarrow{v}$ which will re-focus the target. In our scenario the MIMO system inspects a 200 m $\times$ 300 m area. In this area we are interested in target travelling at around 1.5 m.s^{-1}. If all the Tx were to transmit at the same time the maximum displacement of the target relative to all the transmitted pulses would be in the order of λ/10. Figure 7(b) displays the MIMO image with no transmitting delay of a target moving at 1.5 m.s^{-1}. The target is still well focused.

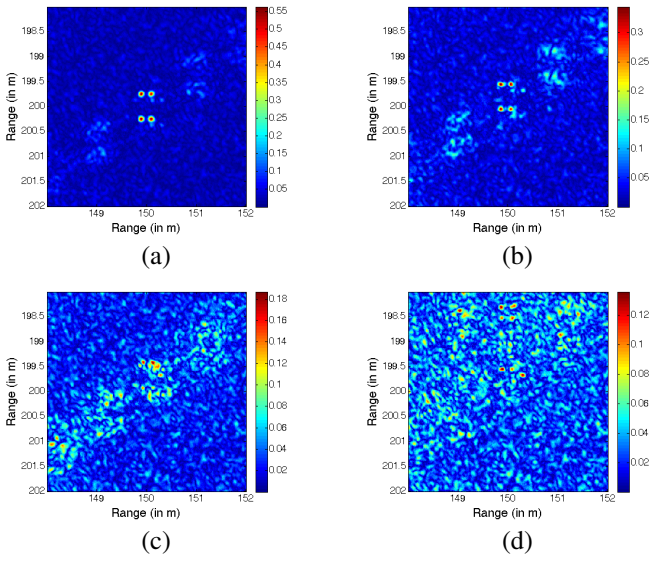

Fig. 7. MIMO image of (a) a static target, (b) moving target with no transmitting delay, (c) moving target with random transmitting delay introducing an average of 4λ/5 target displacement and (d) moving target with random transmitting delay introducing an average of 10λ target displacement.

By introducing random delays to the transmitting pulses we can control the average time difference Δt between pulse times of arrival at the target. The target will then move between two pulses by $\overrightarrow{v}\Delta t$ on average. Figure 7(c) and (d) display the MIMO image of a moving target with random transmitting delay introducing respectively 4λ/5 and 10λ displacement. For a high displacement (greater than λ) the resulting target image is not coherent anymore. For low reflectivity targets the target signal can then be masked by the reverberation level (cf. Figure 7(d)). For an average displacement lower than λ the back projection processing is still coherent and the target structure visible (cf. Figure 7(c)).

From the defocused image and assuming a constant velocity it is possible to compensate the target motion by time shifting the MIMO responses. Let note $z_{kl}(t)$ the signal recorded at the receiver l from the transmitter k. Let note $\Delta_k t$ the transmitting delay of the transmitter k and d_k the distance between transmitter k and the target. The target displacement from $t = 0$ to $t = \delta t = \Delta_k + d_k/c$ time where the pulse transmitted by the transmitter k hit the target is $\overrightarrow{v}\delta t$. The path difference Δ_{kl} between the target location at $t = 0$ and the target location at $t = \delta$ is then:

$$\Delta_{kl}(\overrightarrow{v}) = (\overrightarrow{u_k} + \overrightarrow{u_l}).\overrightarrow{v}\delta t = (\Delta_k + d_k/c)(\overrightarrow{u_k} + \overrightarrow{u_l}).\overrightarrow{v} \quad (15)$$

where $\overrightarrow{u_k}$ and $\overrightarrow{u_l}$ are respectively the direction of arrival and the direction of departure of the sound wave from the target coordinates. Figure 8 draws a schematic of the configuration.

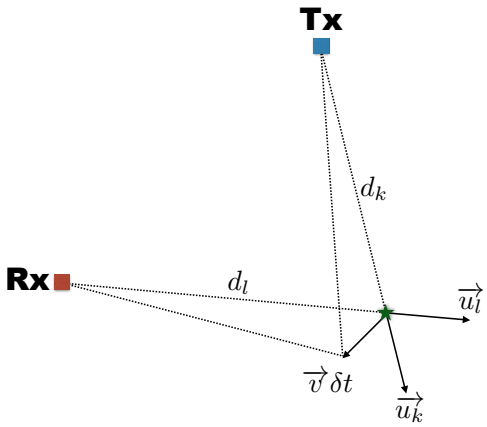

Fig. 8. Schematic and notations: path difference of a moving target.

To focus at a velocity $\overrightarrow{v}$ we then need to compensate for the transmitting time delay and the target motion by applying the multi static back projection algorithm to the set of signals $\left\{z_{kl}(t - \Delta_{kl}(\overrightarrow{v})/c)_{k,l\in[1,K]\times[1,L]}\right\}$ instead of $\left\{(z_{kl}(t))_{k,l\in[1,K]\times[1,L]}\right\}$. The estimated velocity $\overrightarrow{v_e}$ is then given by:

$$\overrightarrow{v_e} = \max_{\overrightarrow{v}}\left[\max\left(\mathrm{BP}\left(\{z_{kl}(t - \Delta_{kl}(\overrightarrow{v})/c)\}_{k,l\in[1,K]\times[1,L]}\right)\right)\right] \quad (16)$$

where BP is the multi static back projection image formation. Figure 9 display the $\max(\mathrm{BP}(\overrightarrow{v}))$ functions for (a) no transmit delay, (b) λ/4 displacement transmit delay and (c)

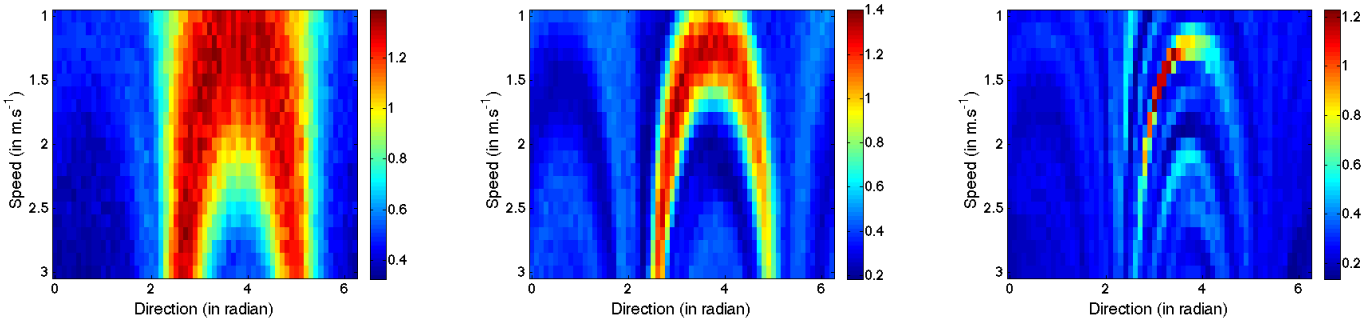

Fig. 9. $\max\left(\mathrm{BP}(v,\theta)\right)$ functions for (a) no transmit delay, (b) $\lambda/4$ displacement transmit delay and (c) $4\lambda/5$ displacement transmit delay. v is the target speed in m.s^{-1} and θ the direction in radian.

$4\lambda/5$ displacement transmit delay. Let note $\overrightarrow{v} = (v, \theta)$ where v is the target speed and θ the target heading.

For no transmit delay or small displacement transmit delay (cf. Figure 9(a) and (b)) the ambiguity between speed and direction is important. In that case the MIMO moving target image was already close to focus and it is not surprising that a large portion of the (v, θ) plane can focus the moving target image. When the displacement transmit delay is important enough to create a defocusing of the moving target (cf. Figure 7(c)) then the optimal focusing value $\overrightarrow{v}$ is a better constraint (cf. Figure 9(c)).

Around 500 tests for speed and direction estimation have be run using this autofocusing technique. Several types of point targets have been tested in different locations with speeds varying from 0.5 m.s^{-1} to 3 m.s^{-1}. In average the speed is estimated with around 0.15 m.s^{-1} error and the heading with around 6° error.

V. Conclusion

Despite the physical constraints, the high number of transmitters and receivers of a large MIMO sonar system gives to the user a great degree of freedom on how to use and exploit large MIMO sonar systems. Assuming independent observations from each MIMO pair we demonstrated that incoherent systems can classify target based on their number of scatterers. We also demonstrated the super-resolution capability of coherent systems that surpasses the state of the art SAS resolution. We presented a physic based MIMO simulator and demonstrated the theoretical results inherent from MIMO sonar systems. A series of techniques based on autofocus algorithms were presented. These techniques allow a large MIMO sonar system in a complex environment to automatically estimate mid water target parameters such as speed or depth and highlight the potential of such sonar system for harbour surveillance.

Acknowledgment

This work was supported by the Engineering and Physical Sciences Research Council (EPSRC) Grant number EP/J015180/1 and the MOD University Defence Research Collaboration in Signal Processing.

References

[1] D. Bliss and K. Forsythe, "Multiple-input multiple-output (mimo) radar and imaging: Degrees of freedom and resolution," in *Proc. 37th Asilomar Conf. Signals, Systems and Computers*, 2003.

[2] E. Fishler, A. Haimovich, R. Blum, J. Cimini, L.J., D. Chizhik, and R. Valenzuela, "Spatial diversity in radars-models and detection performance," *Signal Processing, IEEE Transactions on*, vol. 54, no. 3, pp. 823–838, March 2006.

[3] F. Robey, S. Coutts, D. Weikle, J. McHarg, and K. Cuomo, "Mimo radar theory and experimental results," in *38th Asilomar Conference on Signals, Systems and Computers*, 2004.

[4] N. Lehmann, A. Haimovich, R. Blum, and L. Cimini, "Mimo-radar application to moving target detection in homogenous clutter," in *Adaptive Sensor Array Processing Workshop at MIT Lincoln Laboratory*, 2006.

[5] K. Williams and D. Jackson, "Bistatic bottom scattering: Model, experiments, and model/data comparison," APL-UW, Tech. Rep., 1997.

[6] A. Haimovich, R. Blum, and L. Cimini, "Mimo radar with widely separated antennas," *Signal Processing Magazine, IEEE*, vol. 25, no. 1, pp. 116–129, 2008.

[7] C. Du, Y. Petillot, and J. Thompson, "Predicted detection performance of mimo radar," *Signal Processing Letters, IEEE*, vol. 15, pp. 83–86, 2008.

[8] A. C. Berry, "The accuracy of the gaussian approximation to the sum of independent variates." *Trans. Amer. Math. Soc.*, vol. 49, pp. 122–136, 1941.

[9] Y. Pailhas, "Sonar systems for objects recognition," Ph.D. dissertation, Heriot-Watt University, 2012.

[10] A. Home and G. Yates, "Bistatic synthetic aperture radar," *IEEE RADAR 2002*, pp. 6–10, 2002.

[11] L. Kaplan and C.-C. Kuo, "An improved method for 2-d self-similar image synthesis," *Image Processing, IEEE Transactions on*, vol. 5, no. 5, pp. 754–761, May 1996.

[12] H. Qian, R. Blum, and A. Haimovich, "Noncoherent mimo radar for location and velocity estimation: More antennas means better performance," *Signal Processing, IEEE Transactions on*, vol. 58, no. 7, pp. 3661–3680, July 2010.

[13] A. Hassanien, S. Vorobyov, and A. Gershman, "Moving target parameters estimation in noncoherent mimo radar systems," *Signal Processing, IEEE Transactions on*, vol. 60, no. 5, pp. 2354–2361, May 2012.